Phase-separation propensity of non-ionic amino acids in peptide-based complex coacervation systems

Yuto Akahoshi,[a,b] *Hiroka Sugai*,[a,b] *Masahiro Mimura*,[a,b] *Yoichi Shinkai*,[c] *Ryoji Kurita*,[a,b] *Kentaro Shiraki*,[a] *Shunsuke Tomita*[b,*]

[a] Faculty of Pure and Applied Sciences, University of Tsukuba, 1-1-1 Tennodai, Tsukuba, Ibaraki 305-8573, Japan.

[b] Health and Medical Research Institute, National Institute of Advanced Industrial Science and Technology, 1-1-1 Higashi, Tsukuba, Ibaraki 305-8566, Japan.

[c] Biomedical Research Institute, National Institute of Advanced Industrial Science and Technology, 1-1-1 Higashi, Tsukuba, Ibaraki 305-8566, Japan.

E-mail: s.tomita@aist.go.jp

Abstract

Uncovering the sequence-encoded molecular grammar that governs the liquid–liquid phase separation (LLPS) of proteins is a crucial issue to understand dynamic compartmentalization in living cells and the emergence of protocells. Here, we present a model LLPS system that is induced by electrostatic interactions between anionic nucleic acids and cationic oligolysine peptides modified with 12 different non-ionic amino acids, with the aim of creating an index of 'phase-separation propensity' that represents the contribution of non-ionic amino acids to LLPS. Based on turbidimetric titrations and microscopic observations, the lower critical peptide concentrations where LLPS occurs (C_{crit}) were determined for each peptide. A correlation analysis between these values and known amino-acid indices unexpectedly showed that eight non-ionic amino acids inhibit the generation of LLPS, whereby

the extent of inhibition increases with increasing hydrophobicity of the amino acids. However, three aromatic amino acids deviate from this trend, and rather markedly promote LLPS despite their high hydrophobicity. A comparison with double-stranded DNA and polyacrylic acid revealed that this is primarily due to interactions with DNA nucleobases. Our approach to quantify the contribution of non-ionic amino acids can be expected to help to provide a more accurate description and prediction of the LLPS propensity of peptides/proteins.

Introduction

Liquid–liquid phase separation (LLPS) has attracted great attention as a key thermodynamic process in the dynamic compartmentalization in living cells[1,2] and for the emergence of protocells during the primitive stages of life on earth.[3] In LLPS processes targeted in these contexts, small volumes of molecule-condensed phases (the so-called 'liquid droplets') are formed in dilute bulk phases in aqueous solution. These liquid droplets are water-rich and, unlike hydrogels, usually dense viscoelastic liquids (40–90% water content; 0.1–100 Pa·s viscosity).[4] Important features of these droplets are their rapid, adaptive, and reversible responses to changes in the surrounding environment, such as temperature, pH value, and ionic strength.[5–7] In addition, their permeability due to the absence of a membrane structure allows the selective incorporation of certain molecules with low or high molecular weight, into the interior of the droplet, thereby contributing to the spatiotemporal control of biological reactions.[8,9]

Biological liquid droplets are mainly composed of biomacromolecules such as proteins, DNA, or RNA, among which proteins with intrinsically disordered regions (IDRs) are considered to play fundamental roles in various biological LLPS processes.[4,10] These LLPS

processes are driven by multivalent associative interactions, especially electrostatic, π–π, and cation–π interactions.[11]

Experimental and theoretical approaches have been used in an attempt to uncover the sequence-encoded molecular grammar that governs phase-separation behaviour with respect to IDRs.[12,13] A representative framework is the 'stickers-and-spacers' model, in which attractively interacting 'sticker' residues (e.g., aromatic amino acids), separated by flexible, soluble 'spacer' residues, can lead to the formation of liquid droplets instead of solid aggregates.[14] Sticker residues are not limited to aromatic amino acids, but also include adhesive domain-motif systems and paired charged residues.[15] Most recently, spacer amino acids have also been reported to substantially affect LLPS. For example, the substitution of Gly residues in the spacer region with polar amino acids, such as Ser, Asn, and Gln, destabilizes the phase-separated state, which is thought to be due to increases in the effective solvation volumes (also referred to as the excluded volume) of the peptide chain.[10,16] However, little light has so far been shed on the role of these non-aromatic and non-charged amino-acid residues, albeit that there is little doubt that a systematic comparison and empirical indexing of amino acids, including bulky aliphatic amino acids, which play a critical role in protein folding but have not yet been well addressed in the field of LLPS, will be significant in providing a more accurate description and prediction of biological LLPS.

In this study, we propose a model system based on LLPS triggered by electrostatic interactions between oppositely charged peptides and nucleic acids, with the aim of creating a new index for non-ionic amino acids in LLPS. Electrostatically driven LLPS, which is also known as 'complex coacervation', occurs via the mixing of oppositely charged molecules, such as biomacromolecules (e.g., peptides, proteins, and nucleic acids) and synthetic polymers. This is one of the mechanisms thought to underlie various membrane-less organelles and biomolecular condensates in eukaryotic cells[17–19] and is often the model of choice for protocell studies.[3,20] We have also recently used this LLPS mechanism to understand the role of the

structural features of DNAs in LLPS,[21,22] to elucidate the compartmentalization of enzymes into droplets and its effect on sequential enzyme reactions,[23] and to facilitate the preparation of high-concentration protein solutions for use in protein formulations.[24,25]

Here, as scaffolds for complex coacervation, we selected cationic peptides modified with various non-ionic amino acids and DNA of different sequences. Correlation analyses of the critical peptide concentrations where LLPS occurs with the known amino-acid indices revealed (i) that non-ionic amino acids have an inhibitory effect on LLPS, which increases with increasing side-chain hydrophobicity and (ii) that aromatic amino acids deviate from this trend and instead promote LLPS despite their high hydrophobicity.

Results and discussion

Design of a model LLPS system

To create a system to examine the effects of non-ionic amino acids on LLPS, 12 sequences (K7X3) were designed in which a repeated tripeptide block of a non-ionic amino acid (X3) is attached at the C-terminus of a hepta-lysine peptide (K7; Fig. 1a). The protonated amino groups of the lysine moiety are able to engage in attractive interactions with anionic phosphate groups of DNA. As indicated previously,[26–28] the multivalency of these peptides confers the ability to sufficiently induce LLPS via mixing with DNA, despite their short length, which allows them to be readily synthesized chemically. A circular dichroism (CD) spectroscopical analysis revealed that all 12 peptides exhibit random coil structures under neutral conditions (pH = 7.0), i.e., the influence of the higher-order structure of the peptides can be neglected (Fig. S1). For the nucleic acid, a simple homopolymeric single-stranded DNA (ssDNA) (15-unit repeating deoxyadenylic acid; dA15) was initially chosen.

These peptides and this ssDNA were mixed in various concentration ratios and then observed using optical microscopy to examine whether LLPS occurred. The experimental phase diagram

of K7G3 and dA15 in 50 mM *N*-(2-hydroxyethyl)piperazine-*N*′-2-ethanesulfonic acid (HEPES) buffer (pH = 7.0) in the presence of 10% polyethylene glycol (PEG) showed that droplet-like condensates formed only at K7G3 concentrations above 40 μM and within a specific dA15 concentration range (Fig. 1b). This is known as 're-entrant liquid condensation', which is a phenomenon driven by electrostatic attraction between oppositely charged polyelectrolytes.[29,30] Based on this result, we expected that the contributions of the individual side chains of amino acids could be quantitatively evaluated by determining the minimum peptide concentration where droplets are generated and comparing these values to the case of K7G3, which incorporates Gly residues with no side chains. It should be noted here that amorphous aggregates were not observed under the applied conditions.

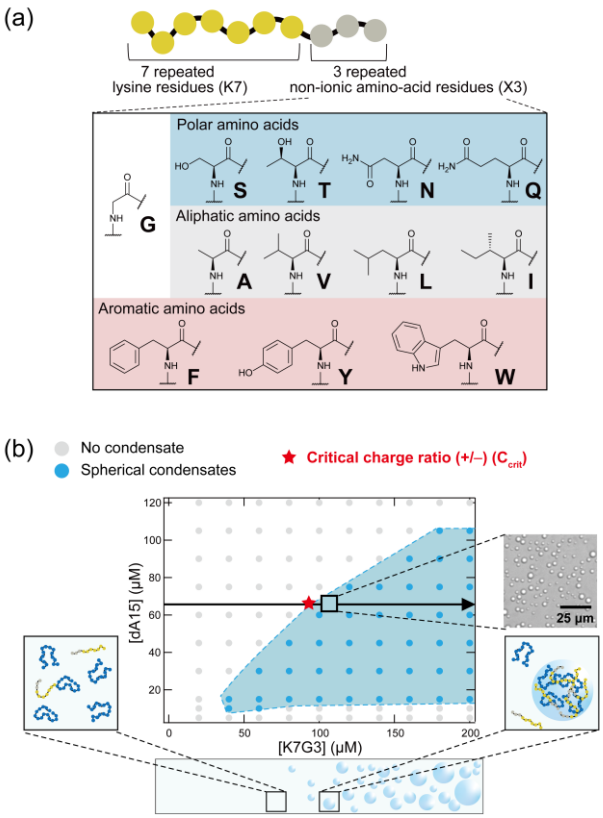

Fig. 1 Peptide/DNA LLPS system designed to investigate the contribution of non-ionic amino acids. (a) Peptides used in this study. (b) Experimental phase diagram of the K7G3 concentration vs. that of dA15. The light blue region indicates the apparent LLPS region. A typical bright field micrograph of K7G3/dA15 droplets is shown on the right. Along the black arrow, the peptide concentration increases progressively at a fixed dA15 concentration. The peptide concentration at the point crossing the phase boundary for a gradually increasing K7G3 concentration and constant dA15 concentration was defined as the critical charge ratio (C_{crit}). All experiments were carried out in 50 mM HEPES (pH = 7.0) and 10% PEG.

Not only K7G3, but also all the other K7X3 peptides, formed droplet-like condensates when mixed with dA15 at concentrations with equal charge ratios (+/−); the charge ratios were calculated as $n_+ x_+ / n_- x_-$, where n is the molar amount of the polymer in solution and x is the number of charges per polymer molecule (Fig. 2a). Time-lapse images showed the sub-millisecond fusion of two adjacent condensates (Fig. 2b for K7G3; see Fig. S2a for representative peptides: K7Y3 with aromatic side chains, K7S3 with hydrophilic side chains, and K7L3 with aliphatic side chains). Considering previous reports,[6,21,22,30,31] this behaviour confirmed that the observed condensates were not solid aggregates but liquid droplets with highly fluidic properties.

To further investigate the liquid properties of the droplets, we carried out fluorescence recovery after photobleaching (FRAP) experiments, a method commonly used to measure the mobility of molecules inside droplets.[6,30,31] Even when dA15 labelled with fluorescein (dA15-FAM) was used instead of dA15, liquid droplets were formed at a charge ratio of 1.0 (+/−) in all four representative peptides, and in all cases dA15-FAM was highly enriched within the droplets (Fig. 2c for K7G3; see Fig. S2c for K7Y3, K7S3, and K7L3). When a portion of a liquid droplet was photobleached, the fluorescence intensity of dA15-FAM recovered over time and reached a plateau within 20 s (Figs. 2c and S2c). The recovery times follow the order K7Y3 > K7S3 > K7G3 ≈ K7L3 (Fig. 2c). These differences suggest that the tripeptides attached to K7 modulate the mode of interaction with dA15, e.g., via hydrogen bonds for Ser and Tyr residues and via π–π interactions for Tyr residues, resulting in a decrease in the mobility of dA15.

Role of non-ionic amino acids in the formation of droplets with ssDNA

After confirming that the designed cationic peptides form liquid droplets with anionic dA15, we subsequently compared the contribution of non-ionic amino acids to the generation of droplets. To quantify the effect of the tripeptides (X3) attached to K7 on the LLPS threshold, the solution turbidity was monitored upon titration of K7X3 with a dA15 solution (Fig. 2d). The charge ratio where the turbidity began to increase was defined as the critical charge ratio (C_{crit}) in the present LLPS system (Fig. 1b). For example, a lower C_{crit} value relative to that of K7G3 indicates that a lower concentration of the peptide is required to induce LLPS, i.e., that the attached non-ionic amino acids promote this phenomenon. Turbidity measurements revealed that all the K7X3 peptides exhibit a constant low turbidity followed by a sharp increase in turbidity above a certain charge ratio (Fig. 2d). Interestingly, the C_{crit} values of the K7X3 peptides (0.35-0.98) depend on the attached amino acid (Fig. 2e), indicating that the

non-ionic amino acid repeats affect the generation of LLPS with dA15. Consistent with these results, we microscopically confirmed the absence/presence of droplets just below/above the C_{crit} values (Fig. S2d).

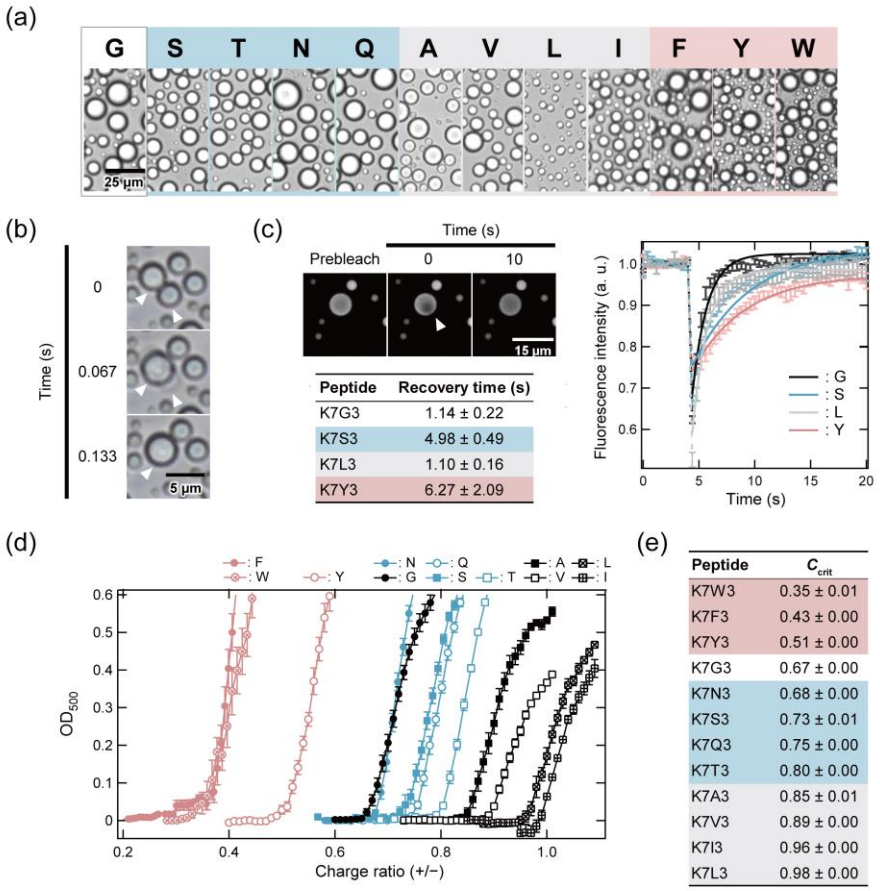

Fig. 2 Role of non-ionic amino acids in the formation of droplets with ssDNA. (a) Bright-field micrographs of K7X3/dA15 solutions with a charge ratio of 1.0 (+/−). The sample solutions contain 67 μM dA15 and 143 μM K7X3. (b) Coalescence of K7G3/dA15 droplets. White arrowheads indicate coalescing droplets. (c) FRAP measurements of representative peptides; left: Confocal fluorescence microscopy images during the FRAP measurement of a K7G3/dA15-FAM droplet. White arrowheads indicate the bleached area; right: FRAP recovery curves for the droplets; values shown represent mean values ± standard error (n = 5). The table below lists the fluorescence recovery times calculated by single-exponential fitting. (d) Turbidimetric titration of K7X3 into the dA15 solution. The optical density at 500 nm (OD_{500}) when K7X3 was titrated into a solution containing 67 μM dA15 is shown. (e) C_{crit} values for K7X3/dA15 solutions determined from panel (d).

To understand why the C_{crit} values were affected by non-ionic amino acids, we compared these values to various amino-acid indices. The C_{crit} values exhibited poor correlations with the general amino-acid index $\log P_{ow}$ (octanol–water partition coefficient according to the

PubChem database; $r = -0.224$; Fig. 3a), the hydropathy index[32] ($r = 0.448$; Fig. 3b), the van der Waals volume[33] ($r = -0.417$; Fig. 3c), and the water solubility[34] ($r = 0.138$, Fig. S3), while the aromaphilicity index, which is determined based on the affinity of the side chains of the amino acids toward aromatic carbon surfaces,[35] exhibited a relatively high negative correlation with the C_{crit} values ($r = -0.803$; Fig. 3d). Based on the distribution of the data points, this high correlation coefficient is apparently due to the K7X3 peptides that contain aromatic amino acids (X = F, Y, and W). A reverse-phase HPLC analysis showed that the overall hydrophobicity of the peptides K7X3 did not differ markedly between those with aromatic and aliphatic side chains (Fig. S4), which suggests that the high LLPS-promoting ability of the aromatic amino acids cannot simply be explained by hydrophobicity. Such specific effects of aromatic amino acids have also been observed in the LLPS of proteins with IDRs.[11,16]

Importantly, when the aromatic amino acids were excluded, the C_{crit} values show a highly positive correlation with indices related to amino-acid hydrophobicity, especially $\log P_{ow}$ ($r = 0.930$; dashed line in Fig. 3a), i.e., the propensity to form liquid droplets decreases with increasing hydrophobicity of the amino acid. This trend is consistent even when amino acids of the same type were compared; the C_{crit} values of Gln, Thr, Val, Ile, and Leu were higher than those of amino acids with fewer methylene/methyl groups, i.e., lower hydrophobicity (Fig. 3e). It should also be noted here that the C_{crit} values were also positively correlated to some extent with the van der Waals volume of the side chain ($r = 0.659$; dashed line in Fig. 3c). According to the stickers-and-spacers model, amino-acid substitutions that increase the effective solvation volumes of the peptide chains destabilize the phase-separated state.[16] Thus, the hydrophobicity and/or steric demand of the side chains (which are correlated) may account for the observed destabilizing effect. Another important point is that this framework can also be applied to hydrophobic aliphatic amino acids, such as Val, Ile, and Leu, in our complex coacervation system. The suppressive behaviour of these hydrophobic aliphatic amino acids, which appears to be contrary to their general classification as promotors of folding and

aggregation,[36] may be related, for example, to the clathrate water, as the clathrate water formed around hydrophobic regions inhibits intermolecular association.[37] Consequently, elastin-like IDR peptides inhibit lower critical solution temperature (LCST)-type LLPS behaviour, and higher hydrophobicity corresponds to reduced likelihood of LLPS.[38]

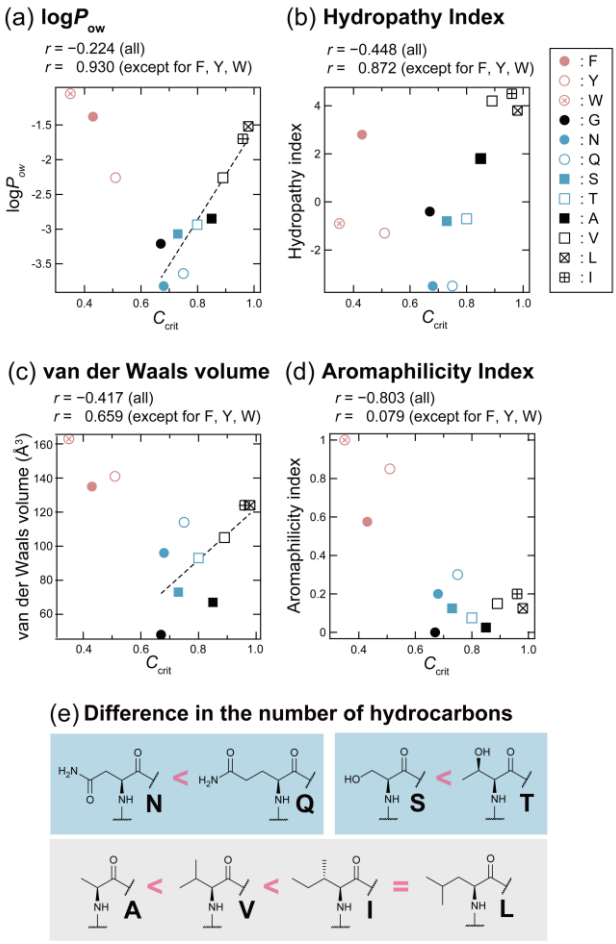

Fig. 3 Comparison of the C_{crit} values for K7X3/dA15 solutions and known amino-acid indices. Plots of the C_{crit} values vs. (a) logP_{ow}, (b) hydropathy index, (c) van der Waals volume, and (d) aromaphilicity index of each amino acid. (e) Difference in the number of hydrocarbons in the side chains of each amino acid.

In summary, we have discovered that in the complex coacervation between K7X3 and dA15, (i) the addition of side chains that contain more hydrophobic (or bulkier) hydrocarbons to the amino acid X inhibits LLPS, whereas (ii) the addition of hydrophobic and bulky aromatic side chains specifically promotes LLPS over the negative effect of the side chains. In general, the

addition of hydrophobic amino acids makes proteins more prone to aggregation (or liquid–solid phase separation);[36] thus, it is surprising that they instead suppress liquid-like condensation (or liquid–liquid phase separation) in the case of this complex-coacervation system.

Generality and mechanism of the effects of non-ionic amino acids on LLPS

The generality of the contribution of non-ionic amino acids was examined using ssDNA with a mixed-base sequence in the linker DNA (5′-GCATG TGGAT CCGAA-3′; dR15).[39] When various concentrations of K7X3 were added to 67 μM dR15, liquid droplets were observed above a certain concentration in all seven representative K7X3 peptides (Fig. S5), as well as dA15. The range of C_{crit} values for K7X3/dR15 was roughly estimated based on bright-field microscopy images and compared with those of dA15 (Figs. 4a and S5). dR15 and dA15 showed a similar trend, i.e., compared with K7G3, aromatic amino acids promoted LLPS, while the other amino acids suppressed LLPS increasingly with increasing hydrophobicity. Thus, the effects of non-ionic amino acids are likely to be common regardless of the sequence of the ssDNA.

While the phase-separation propensity of non-ionic amino acids followed an order similar to that of the ssDNA, we questioned whether this would be common to other complex-coacervation systems and why the behaviour of aromatic amino acids differs from that of the others. Thus, we attempted to gain more insight into its generality and mechanism using (i) double-stranded DNA (dsDNA) and (ii) polyacrylic acid (PAA), an anionic synthetic polymer.

π–π Interactions between the side chain of aromatic amino acids and nucleobases contribute to the formation of droplets between proteins and nucleic acids.[21,22,40] The nucleobases are embedded in the dsDNA of dR15 and its complementary strand (dsDNA15) due to base pairing, thus preventing access of the peptides to the nucleobases. Therefore, we assumed that dsDNA15 could be used to examine the effect of the nucleobases. Mixing of K7X3 and

dsDNA15 resulted in the formation of droplet-like condensates, at least in the lower concentration range (Fig. S6). The order of the estimated regions of C_{crit} for five K7X3 peptides (X = G, N, T, A, and L) did not change significantly from that for the ssDNAs, albeit that Trp and Phe exhibited a relative decrease in their promoting effects (Fig. 4b). Considering the differences in the hydrophobicity of the peptides (Fig. S4), aromatic amino acids still preferentially induce LLPS compared to aliphatic amino acids. This may be due to the unstable end portions of the short dsDNA with partial exposure of the nucleobases.[41]

To strictly exclude the potential contribution of heteromolecular π–π interactions, we next used PAA without aromatic heterocycles. The order of five of the K7X3 peptides (X = G, N, T, A, and L) was again consistent with those for the DNAs (Figs. 4c, and S7), indicating a common action of non-ionic amino acids on complex coacervation systems. Significantly, the effects of Trp and Phe on LLPS were further decreased compared to the case of dsDNA15, and both exert a rather suppressive effect compared to Gly (Fig. 4c). The marked decrease in the ability of aromatic amino acids to induce LLPS should be attributed to the lack of π–π interacting moieties in the counter anionic polyelectrolytes. However, the LLPS ability of the aromatic amino acids remained high given their hydrophobicity (Fig. S4). In the case of aromatic amino acids, interactions among the peptides may contribute to the promotion of LLPS. Examples include π–π interactions between aromatic rings[17] and cation–π interactions between aromatic rings and Lys side chains.[42] We therefore concluded that the negative effect of high hydrophobicity of K7W3 and K7F3 was counterbalanced by the positive effect of interactions among the peptides, resulting in a phase-separation potential similar to that of K7A3 and K7L3, respectively.

The generality of the observed effect of the amino acids, other than aromatic amino acids, on complex coacervation systems, was unexpected. Although hydrophobic aliphatic amino acids attract each other to drive protein folding and aggregation,[36] the tripeptide segments of

these amino acids would not have been net attractive in the current system, and thereby did not promote assembly compaction.

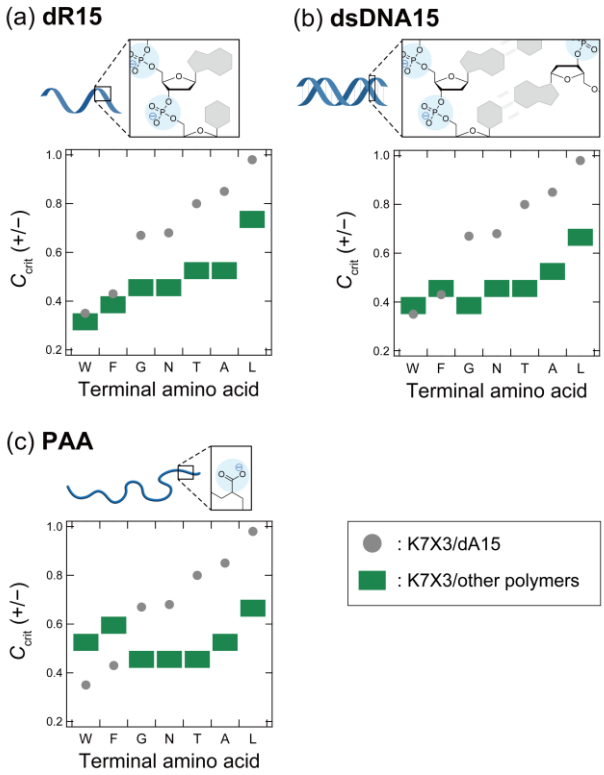

Fig. 4 Comparison between the C_{crit} values for K7X3/dA15 and those for K7X3/other polymers. Filled circles indicate the C_{crit} values for K7X3/dA15 solutions determined from the turbidimetric titrations shown in Fig. 2. Green bars indicate the estimated C_{crit} region for (a) K7X3/dR15, (b) K7X3/dsDNA15, and (c) K7X3/PAA solutions, which were derived from the bright-field microscopy images in Figs. S5–S7. Samples contain (a) 40–130 μM K7X3 and 67 μM dR15; (b) 30–130 μM K7X3 and 33 μM dsDNA15; (c) 60–130 μM K7X3 and 94 μg/mL PAA (1 mM in monomer units); in 50 mM HEPES (pH = 7.0) and 10% PEG.

Role of non-ionic amino acids in an environment closer to physiological conditions

Finally, we examined whether the findings of this study are maintained in an environment closer to physiological conditions, i.e., in conditions of high salt concentrations and high crowding. The addition of various concentrations of K7X3 to a higher concentration of dA15 (200 μM) induced the formation of liquid droplets in the presence of 20% PEG (Fig. S8). The estimated C_{crit} regions of K7X3/dA15 followed an order similar to that under low ionic strength, albeit that the difference in the maximum (K7L3) and minimum (K7W3) C_{crit} values increased

from 2.8-fold to about 12-fold (Fig. 5). Since the addition of high concentrations of PEG is used to reproduce crowded cellular environments,[43] the effects of the non-ionic amino acids that we observed are likely to act as regulators of LLPS in cells.

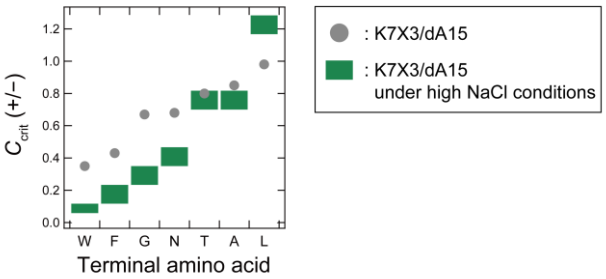

Fig. 5 Comparison between the C_{crit} values for K7X3/dA15 and those for K7X3/dA15 under high NaCl conditions. Filled circles indicate the C_{crit} values for K7X3/dA15 solutions derived from the turbidimetric titrations in Fig. 2. Green bars indicate the estimated C_{crit} region for K7X3/dA15 with NaCl derived from the bright-field microscopy images in Fig. S8. Samples contain 25–550 μM K7X3, 200 μM dA15, 100 mM NaCl, 50 mM HEPES (pH = 7.0), and 20% PEG.

Conclusions

In summary, we have created a peptide-based model for complex coacervation systems and used it to discover that (i) non-ionic amino acids inhibit LLPS, whereby the inhibitory effect increases with increasing hydrophobicity, and that (ii) hydrophobic aromatic amino acids do not follow this rule, but instead promote LLPS. The LLPS-promoting ability of the aromatic amino acids was attributed to the interactions with the aromatic moieties of the anionic polyelectrolytes, and therefore, the effects varied depending on the partner structures. The experimentally determined C_{crit} values can potentially be used to quantitatively account for the contribution of non-ionic amino acids to LLPS, especially in complex coacervation systems. Although we found that the order of the C_{crit} values of non-ionic amino acids, except in the case of aromatic amino acids, is almost independent of the counterionic polyelectrolytes (ssDNA, dsDNA, or synthetic PAA), it is still unclear whether the present results are valid for other peptide arrangements, systems involving aggregate formation, or the so-called simple coacervation systems,[3] which are frequently observed in IDRs such as hnRNAP1[14,16] and fused in sarcoma (FUS).[44]

Extensive further studies including these systems should make this phase-separation propensity index more robust. These efforts will provide fundamental insights in order to facilitate the understanding and prediction of biological LLPS and to support the design of protocells and the discussion of their emergence.

Author Contributions

Conceptualization: Y. A., H. S., M. M., K. S., and S. T.; funding acquisition: H. S., K. S., and S. T.; data curation and formal analysis: Y.A.; investigation: Y. A. and Y. S.; methodology: Y. A., H. S., M. M., and S. T.; resources: Y. S., R. K., K. S., and S. T.; visualization: Y. A. and H. S.; supervision: S. T.; writing – original draft: Y. A., H. S., and S. T.; writing – review & editing: all authors.

Conflicts of interest

The authors declare no competing interests.

Acknowledgements

This research was partially supported by JSPS KAKENHI grants JP18H02383 and JP19K22377 (to K. S. and S. T.), JP21K20622 (to H. S.), and AMED under grant number JP21wm0425004 (to S. T.).

Notes and references

1 S. F. Banani, H. O. Lee, A. A. Hyman and M. K. Rosen, *Nat. Rev. Mol. Cell Biol.*, 2017, **18**, 285–298.

2 S. Alberti, *J. Cell Sci.*, 2017, **130**, 2789–2796.

3 M. Abbas, W. P. Lipiński, J. Wang and E. Spruijt, *Chem. Soc. Rev.*, 2021, **50**, 3690–3705.

4 N. A. Yewdall, A. A. M. André, T. Lu and E. Spruijt, *Curr. Opin. Colloid Interface Sci.*, 2021, **52**, 101416.

5 T. J. Nott, E. Petsalaki, P. Farber, D. Jervis, E. Fussner, A. Plochowietz, T. D. Craggs, D. P. Bazett-Jones, T. Pawson, J. D. Forman-Kay and A. J. Baldwin, *Mol. Cell*, 2015, **57**, 936–947.

6 S. Alberti, A. Gladfelter and T. Mittag, *Cell*, 2019, **176**, 419–434.

7 G. Krainer, T. J. Welsh, J. A. Joseph, J. R. Espinosa, S. Wittmann, E. de Csilléry, A. Sridhar, Z. Toprakcioglu, G. Gudiškytė, M. A. Czekalska, W. E. Arter, J. Guillén-Boixet, T. M. Franzmann, St Qamar, P. S. George-Hyslop, A. A. Hyman, R. Collepardo-Guevara, S. Alberti and T. P. J. Knowles, *Nat. Commun.*, 2021, **12**, 1085.

8 T. J. Nott, T. D. Craggs and A. J. Baldwin, *Nat. Chem.*, 2016, **8**, 569–575.

9 J. A. Ditlev, L. B. Case and M. K. Rosen, *J. Mol. Biol.*, 2018, **430**, 4666–4684.

10 J.-M. Choi, A. S. Holehouse and R. V. Pappu, *Annu. Rev. Biophys.*, 2020, **49**, 107–133.

11 C. P. Brangwynne, P. Tompa and R. V. Pappu, *Nat. Phys.*, 2015, **11**, 899–904.

12 J. Wang, J.-M. Choi, A. S. Holehouse, H. O. Lee, X. Zhang, M. Jahnel, S. Maharana, R. Lemaitre, A. Pozniakovsky, D. Drechsel, I. Poser, R. V. Pappu, S. Alberti and A. A. Hyman, *Cell*, 2018, **174**, 688-699.e16.

13 E. W. Martin and T. Mittag, *Biochemistry*, 2018, **57**, 2478–2487.

14 E. W. Martin, A. S. Holehouse, I. Peran, M. Farag, J. J. Incicco, A. Bremer, C. R. Grace, A. Soranno, R. V. Pappu and T. Mittag, *Science*, 2020, **367**, 694–699.

15 W. Borcherds, A. Bremer, M. B. Borgia and T. Mittag, *Curr. Opin. Struct. Biol.*, 2021, **67**, 41–50.

16 A. Bremer, M. Farag, W. M. Borcherds, I. Peran, E. W. Martin, R. V. Pappu and T. Mittag, *Nat. Chem.*, 2022, **14**, 196–207.

17 C. W. Pak, M. Kosno, A. S. Holehouse, S. B. Padrick, A. Mittal, R. Ali, A. A. Yunus, D. R. Liu, R. V. Pappu and M. K. Rosen, *Mol. Cell*, 2016, **63**, 72–85.

18 V. N. Uversky, *Adv. Colloid Interface Sci.*, 2017, **239**, 97–114.

19 T. Ukmar-Godec, S. Hutten, M. P. Grieshop, N. Rezaei-Ghaleh, M.-S. Cima-Omori, J. Biernat, E. Mandelkow, J. Söding, D. Dormann and M. Zweckstetter, *Nat. Commun.*, 2019, **10**, 2909.

20 B. Ghosh, R. Bose and T.-Y. D. Tang, *Curr. Opin. Colloid Interface Sci.*, 2021, **52**, 101415.

21 M. Mimura, S. Tomita, Y. Shinkai, T. Hosokai, H. Kumeta, T. Saio, K. Shiraki and R. Kurita, *J. Am. Chem. Soc.*, 2021, 143, 9849–9857.

22 M. Mimura, S. Tomita, H. Sugai, Y. Shinkai, S. Ishihara and R. Kurita, *Front. Cell. Dev. Biol.*, 2021, **9**, 710729.

23 T. Ura, S. Tomita and K. Shiraki, *Chem. Commun.*, 2021, **57**, 12544–12547.

24 A. Matsuda, M. Mimura, T. Maruyama, T. Kurinomaru, M. Shiuhei and K. Shiraki, *J. Pharm. Sci.*, 2018, **107**, 2713–2719.

25 K. Tsumura, W. Hsu, M. Mimura, A. Horiuchi and K. Shiraki, *J. Biosci. Bioeng.*, 2022, **133**, 17–24.

26 S. Koga, D. S. Williams, A. W. Perriman and S. Mann, *Nat. Chem.*, 2011, **3**, 720–724.

27 T.-Y. D. Tang, M. Antognozzi, J. A. Vicary, A. W. Perriman and S. Mann, *Soft Matter*, 2013, **9**, 7647–7656.

28 F. P. Cakmak, S. Choi, M. O. Meyer, P. C. Bevilacqua and C. D. Keating, *Nat. Commun.*, 2020, **11**, 5949.

29 P. R. Banerjee, A. N. Milin, M. M. Moosa, P. L. Onuchic and A. A. Deniz, *Angew. Chem., Int. Ed.*, 2017, **56**, 11354–11359.

30 I. Alshareedah, T. Kaur, J. Ngo, H. Seppala, L.-A. D. Kounatse, W. Wang, M. M. Moosa and P. R. Banerjee, *J. Am. Chem. Soc.*, 2019, **141**, 14593–14602.

31 S. Elbaum-Garfinkle, Y. Kim, K. Szczepaniak, C. C.-H. Chen, C. R. Eckmann, S. Myong and C. P. Brangwynne, *Proc. Natl. Acad. Sci. U. S. A.*, 2015, **112**, 7189–7194.

32 J. Kyte and R. F. Doolittle, *J. Mol. Biol.*, 1982, **157**, 105–132.

33 T. E. Creighton, *Protein structure: a practical approach*, Oxford University Press, 1993.

34 J. P. Amend and H. C. Helgeson, *Pure Appl. Chem.*, 1997, **69**, 935–942.

35 A. Hirano and T. Kameda, *ACS Appl. Nano Mater.*, 2021, **4**, 2486–2495.

36 A. L. Fink, *Fold. Des.*, 1998, **3**, R9-23.

37 G. C. Yeo, F. W. Keeley and A. S. Weiss, *Adv. Colloid Interface Sci.*, 2011, **167**, 94–103.

38 M. Miao, C. M. Bellingham, R. J. Stahl, E. E. Sitarz, C. J. Lane and F. W. Keeley, *J. Biol. Chem.*, 2003, **278**, 48553–48562.

39 M. V. Bass, T. Nikitina, D. Norouzi, V. B. Zhurkin and S. A. Grigoryev, *J. Biol. Chem.*, 2019, **294**, 4233–4246.

40 I. Alshareedah, M. M. Moosa, M. Pham, D. A. Potoyan and P. R. Banerjee, *Nat. Commun.*, 2021, **12**, 6620.

41 I. Ferreira, T. D. Amarante and G. Weber, *J. Chem. Phys.*, 2015, **143**, 175101.

42 S. Park, S. Kim, Y. Jho and D. S. Hwang, *Langmuir*, 2019, **35**, 16002–16012.

43 A. A. M. André and E. Spruijt, *Int. J. Mol. Sci.*, 2020, **21**, 5908.

44 A. Patel, H. O. Lee, L. Jawerth, S. Maharana, M. Jahnel, M. Y. Hein, S. Stoynov, J. Mahamid, S. Saha, T. M. Franzmann, A. Pozniakovski, I. Poser, N. Maghelli, L. A. Royer, M. Weigert, E. W. Myers, S. Grill, D. Drechsel, A. A. Hyman and S. Alberti, *Cell*, 2015, **162**, 1066–1077.